Late Quaternary left-lateral strike slip rate along the Anninghe–Zemuhe Section of the Xianshuihe–Xiaojiang Fault System and its implication to the clockwise block rotation of the SE margin of the Tibetan Plateau

Mengmeng Hu[1,2], Zhonghai Wu[1]*, Jiacun Li[3], Keqi Zhang[1], Klaus Reicherter[4], Wenjun Bi[5]

[1] Key Laboratory of Neotectonic Movement and Geohazard, The Institute of Geomechanics, Chinese Academy of Geological Sciences, Beijing 100081, China.

[2] School of Earth and Space Sciences, Peking University, Beijing 100871, China.

[3] Key Laboratory of 3D Information Acquisition and Application, MOE, Capital Normal University, Beijing 100048, China.

[4] Neotectonics and Natural Hazards, RWTH Aachen University, Lochnerstr. 4–20, 52056 Aachen, Germany.

[5] School of Earth Sciences and Resources, China University of Geosciences, Beijing 100083, China.

Corresponding author: Zhonghai Wu (wuzhonghai8848@foxmail.com)

Key Points:

- The late Quaternary sinistral strike-slip rates of Anninghe Fault and Zemuhe Fault were constrained to be 6.9 ±0.6 mm/a and 11.2 ±0.4 mm/a, respectively.
- The late Quaternary slip rate of the Xianshuihe–Xiaojiang Fault System is roughly uniform along the strike, with a value of 12–15 mm/a.
- The uniform high-speed strike-slip along the Xianshuihe–Xiaojiang Fault System largely constrains the clockwise rotation of the SE margin of the Tibetan Plateau.

Abstract

Crustal material eastward extrusion from the Tibetan Plateau is closely related to the strike-slip faults in the SE margin of the Tibetan Plateau. The left-lateral strike-slip Xianshuihe–Xiaojiang fault system (XXFS) is the most active and the largest-scale one. The slip rates along the XXFS is crucial for unraveling the kinematics of the SE margin of the Tibetan Plateau. The central section of the XXFS, also known as the Anninghe–Zemuhe section, was poorly researched owing to its inaccessibility, a lack of high-quality quantitative age data, as well as questionable displacement determination and methodology. In this study, we adopted high-resolution topographic data (terrestrial laser scanning) and high-accuracy dating methods (OSL and 14C) to obtain more reliable slip rates of Anninghe Fault and Zemuhe Fault. The late Quaternary slip rates of Anninghe Fault and Zemuhe Fault were constrained to be 6.9±0.6 mm/a and 11.2±0.4 mm/a, respectively. A large of rate statistics was also conducted along the XXFS. We found that the slip rate of the XXFS is in a narrow range of 12–15 mm/a (slightly increasing from north to south) after taking the Daliangshan Fault into account. Combined with the analysis of the relationship between the active faults and block rotation, we proposed that the uniform high-speed strike-slip along the XXFS largely constrains the clockwise rotation of the SE margin of the Tibetan Plateau.

Plain language summary

The collision between the Indian Plate and the Eurasian Plate began about 50 to 60 million years ago, when the north-moving Indian Plate, moving at about 50–60 mm per year, collided with the Eurasian Plate. As a result, crustal materials of the Tibetan Plateau either shortened/thickened or extruded out of India's northward path with several orientations. The crustal materials extruded eastward has two main modes owning to the major boundary fault—left-lateral strike-slip Xianshuihe-Xiaojiang Fault System. We focused on the late Quaternary strike-slip rate of this fault to explore its kinematics characterizes for the research of the deformation in SE margin of the Tibetan Plateau results from the collision of the Indian-Eurasian Plate. It is proven that the SE margin of the Tibetan Plateau clockwise rotates under the constraint of the uniform high-speed strike-slip of the Xianshuihe–Xiaojiang Fault System.

1 Introduction

Significant surface deformation has occurred in response to the collision of Indian and Eurasian Plates since 50–65 Ma (Molnar & Tapponnier, 1975; Harrison et al., 1992; Yin & Harrison, 2000; Li et al., 2012). The 50-60 mm/a of convergence between the two plates is partitioned into comparable fractions of convergence at the Himalaya, at the Tien Shan, and across Tibet, with the latter manifested as eastward extrusion of material out of India's northward path (Molnar & Lyon-Caen, 1989). A ~20 mm/a of eastward relative motion with respect to stable Eurasia was observed at the northwest end of the SE margin of the Tibetan Plateau (Zhang et al., 2004). Based on GPS observations, Gan et al. (2007) discovered that the crustal materials of the SE margin of the Tibetan Plateau are inclined to extrude southeastward-southward from NW to SE, with a decrease in the velocity. Lateral slip on the strike-slip faults may be a particularly efficient mechanism to accommodate the extrusion strain, as researched: left-lateral shear on planes with a systematically varying orientation appears to dominate the active strain field across eastern Tibet (Molnar & Lyon-Caen, 1989). Most kinematic models of central Asia take the Red River fault as the major southeastern boundary of the lateral extrusion of the

Tibetan crust (e.g. Armijo et al., 1989; Avouac & Tapponnier, 1993; Leloup et al., 1995, 2001). Moreover, Armijo et al. (1989) described the extrusion of Tibet as the expulsion of a rigid block bounded on the south by the right-lateral shear zone and on the north by the left-lateral Altyn Tagh fault. In addition, clockwise rotations observed by GPS method is proven to take up another part of the extrusion strain (Shen et al., 2005; Gan et al., 2007; Loveless et al., 2011; Zhang, 2013). Two arguments have been summarized for the style of the rotation. Molnar & Lyon-Caen (1989) suspected that the extrusion of eastern Tibet occurs both by left-lateral slip on roughly east-west trending planes and simultaneously by block rotation of the material between the major boundary faults. Xu et al. (2003) proposed that the rotation occurred within the sub-blocks. These sub-blocks are bounded by sets of sub-parallel strike-slip faults, which accommodate the relative motion between the sub-blocks under the simple shear on two boundary faults. Here assumed that each sub-block is approximately rigid, and most of the deformation is localized on the boundary faults, and little deformation occurs within the block. In conclusion, it remains uncertain how the rotation of the SE margin of the Tibetan Plateau is achieved. Determining the kinematics of active faulting will thus provide insight into this question.

A series of major strike-slip faults develop inside or at boundaries of the SE margin of the Tibetan Plateau, including the left-lateral XXFS, Litang Fault, Nantinghe Fault, Wanding Fault, and Lijiang-Xiaojinhe Fault, and the right-lateral Red River Fault and Batang Fault (Wang et al., 1998; Xu et al., 2003). Existing GPS observation and geological results show that the XXFS is the most active one (Shen et al., 2005; Wu & Zhou, 2018). It is also the eastern boundary of the SE margin of the Tibetan Plateau (Wu & Zhou, 2018). The slip rates of the XXFS are crucial for unraveling the kinematics of the SE margin of the Tibetan Plateau. The central section of the XXFS, referring to the Anninghe–Zemuhe section, is poorly researched on the slip rate owing to its inaccessibility, and technical limitations such as low-accuracy dating methods and low-resolution topography data as well as potential inconsistencies between age and displacement data. It thus constrains the exploring of the kinematics of the SE margin of the Tibetan Plateau. Therefore, more reliable slip rates of Anninghe Fault and Zemuhe Fault are needed for resolving this problem.

In this study, we aimed to constrain the Late Quaternary horizontal slip rates of Anninghe Fault and Zemuhe Fault by dating the offsets of the Q_4 Fan edge at the Majiagou (MJG) site and a T2/T3 riser south of it as well as the offset of a terrace scarp at the Wudaoqing (WDQ) site. We then reanalyzed the slip rate of each section of the XXFS along strike by conducting a large of rate statistics. Combined with the analysis of the relationship between the active faults and block rotation, we proposed the kinematics model applicable in the SE margin of the Tibetan Plateau.

2 Tectonics setting

The XXFS formed in the Cenozoic, cutting the pre-Cenozoic tectonic units in the eastern part of the Tibetan Plateau, including the Bayan Har Block in the north, the Yangtze Platform in the southeast, and the Qiangtang Block and the Chuandian Block in the southwest (**Figure 1**; He & Oguchi, 2008; Jiang et al., 2015; Chevalier et al., 2017; Bai et al., 2018). The fault system is distributed in a broken line in the eastern part of Sichuan and Yunnan, forming an arc protruding toward the NE, generally consisting of Xianshuihe fault, Anninghe fault, Zemuhe fault, and Xiaojiang fault.

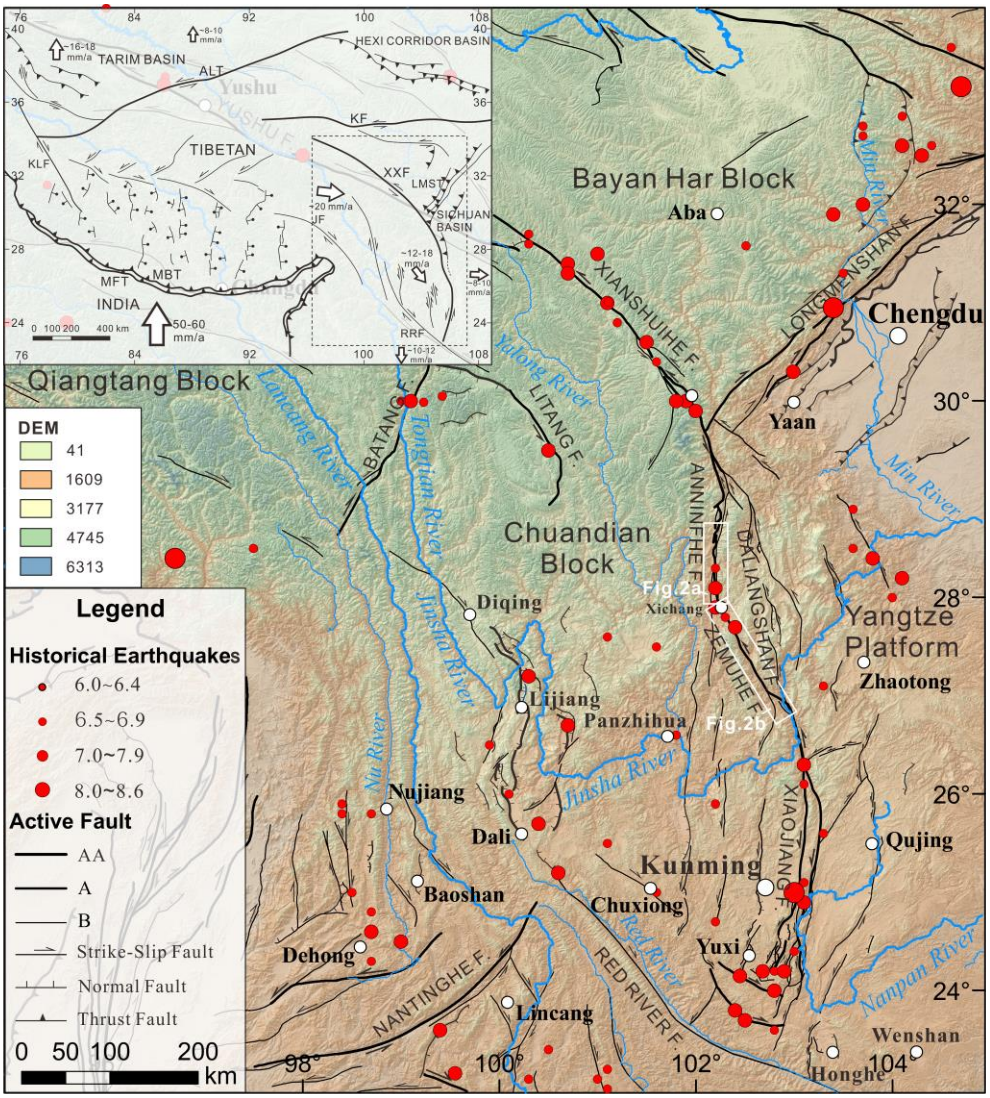

Figure 1. Inset illustrates the location of the SE margin of the Tibetan Plateau. The main figure shows the principal active faults, historical earthquakes with magnitude ≥ 6.0, and rivers in the SE margin of the Tibetan Plateau, mapped on a Digital Elevation Model (SRTMDEM res-90 m). Major towns are also indicated. All data taken from Wu & Zhou (2018).

The Anninghe Fault connects with the NW-trending Xianshuihe Fault near Tianwan, passing southward through Jiziping, Zimakua, Xiaoyanjing, Mianning, Lugu, and Lizhou to Xining, and then connects with the NNW-trending Zemuhe Fault. It generally consists of two branches in the east and west, with a total length of more than 160 km, and the overall trend is approximately NS, with partial sections following a NE or slightly W trend. The west branch is composed of multiple secondary faults, and the activity is dominated by left-lateral strike-slip with a thrust component. At present, it is not active. The east branch is dominated by left-lateral strike-slip with a distinct normal component, and activity in the section to the south of Xichang has gradually weakened. To the north of Xichang, the activity continuously strengthened until the Holocene.

From Zimakua to Xichang, the east branch of Anninghe Fault can be clearly divided into two segments, with the Xiaoyanjing as the center (**Figure 2a**). The northern segment is in an environment dominated by strong uplifting and erosion with obvious characteristics of intermittent extension, and some segments no longer exhibit strong activity. The southern segment, which will be focused in this paper, is composed of two diagonally parallel faults, lying on the eastern edge of the Anninghe depression and the west side of the Xiaoxiangling uplifted fault block. Between them, there is a striped low mountain with a width of 0.7–3 km, a length of approximately 70 km, and an elevation of 2000–2600 m at the highest point. The east and west sides of the low mountain are the main sites for the activity and distribution of the southern segment in the Late Quaternary. The east fault ceased strong activity at the end of the Late Pleistocene to the Early Holocene, while the west fault remains active today. The southern segment is the main location for strong earthquakes. Historical records show that almost all strong earthquakes and the corresponding surface ruptures were concentrated on this segment. In contrast, the northern segment is not inclined to cause strong earthquakes, instead causing weak earthquakes, showing its creeping nature. Accordantly with the segmentation, the late Quaternary strike-slip rate of the Anninghe Fault shows a discrepancy in its two segments. Owing to the inaccessibility of the area, sparse slip rates were gained on the northern segment compared to that on the southern segment. It is suggested to be an average of 3.9 mm/a (Tang et al., 1992; Zhou et al., 2001b; Ran et al., 2008; Cheng, 2010), which is lower than that of the southern segment with a mean value of 4.8 mm/a (Tang et al., 1989, 1992; Qian et al., 1992; Pei et al., 1997; He & Yasutakyr, 2007; Wang et al., 2018). The GPS data indicates a higher slip rate of 6.15 mm/a of the modern period for the entire fault (Shen et al., 2005; Wang et al., 2008;; Loveless & Meade, 2011; Cheng et al., 2011; Zhang, 2013; Wang et al., 2017b; Ma, 2019; Wang & Shen, 2020).

The Zemuhe Fault extends approximately 140 km NNW–SSE from Xichang in the north to Qiaojia in the south (**Figure 2b**). Between Wudaoqing Township and Puge County, it is mainly distributed along the southwest edge of the Zemu River Valley. Passing through Puge County, it extends along the east side of the Heishui River Valley and intersects with the Xiaojiang Fault at the south end of the Qiaojia Basin (Huang & Tang, 1983). It is composed of a series of parallel or nearly parallel faults, forming a fault zone that gradually widens to the northwest, with a width of approximately 7–8 km. Du (2000a) focused on the segmentation of characteristic seismic ruptures, and divided the Zemuhe Fault into five left-step, left-lateral strike-slip faults from northwest to southeast as follows: Li Jinbao Fault, Daqing Fault, Chechejie Fault, Songxin Fault, and Datong Fault. Their lengths are between 20–55 km, mainly inclined to the northeast, and their dip angle is greater than 60°. Six pull-apart basins (viz. Xichang Basin, Tuomugou Basin, Puge Basin, Songxin Basin, Ningnan Basin, and Qiaojia Basin) were developed in the stepovers and the north and south ends of the faults. The average late Quaternary slip rates on the five faults are 6.3, 6.6, 8.1, 6.0, and 4.7 mm/a from north to south (Ren, 1990; He et al., 1999; Du, 2000b; Wang et al., 2011). The modern activity of the fault revealed by GPS measurements shows a coincident result with those presented above (Qiao et al., 2004; Shen et al., 2005; Cheng et al., 2011; Zhang, 2013; Wang et al., 2017b). However, the slip rate since pre-middle Pleistocene can reach up to ~10 mm/a (Du, 2000b). In addition, Songxin Township divides Zemuhe Fault into two segments based on seismic segmentation. Five documented earthquakes with magnitude greater than M5 occurred in the northern segment, especially near Xichang. The southern segment is characterized by many weak earthquakes, which mainly occurred near Ningnan to Qiaojia. We mainly discussed the slip rate of the Daqing Fault, where the dislocation geomorphology is the most developed, and the earthquake events revealed by the ancient earthquake and historical earthquake records are also the most abundant.

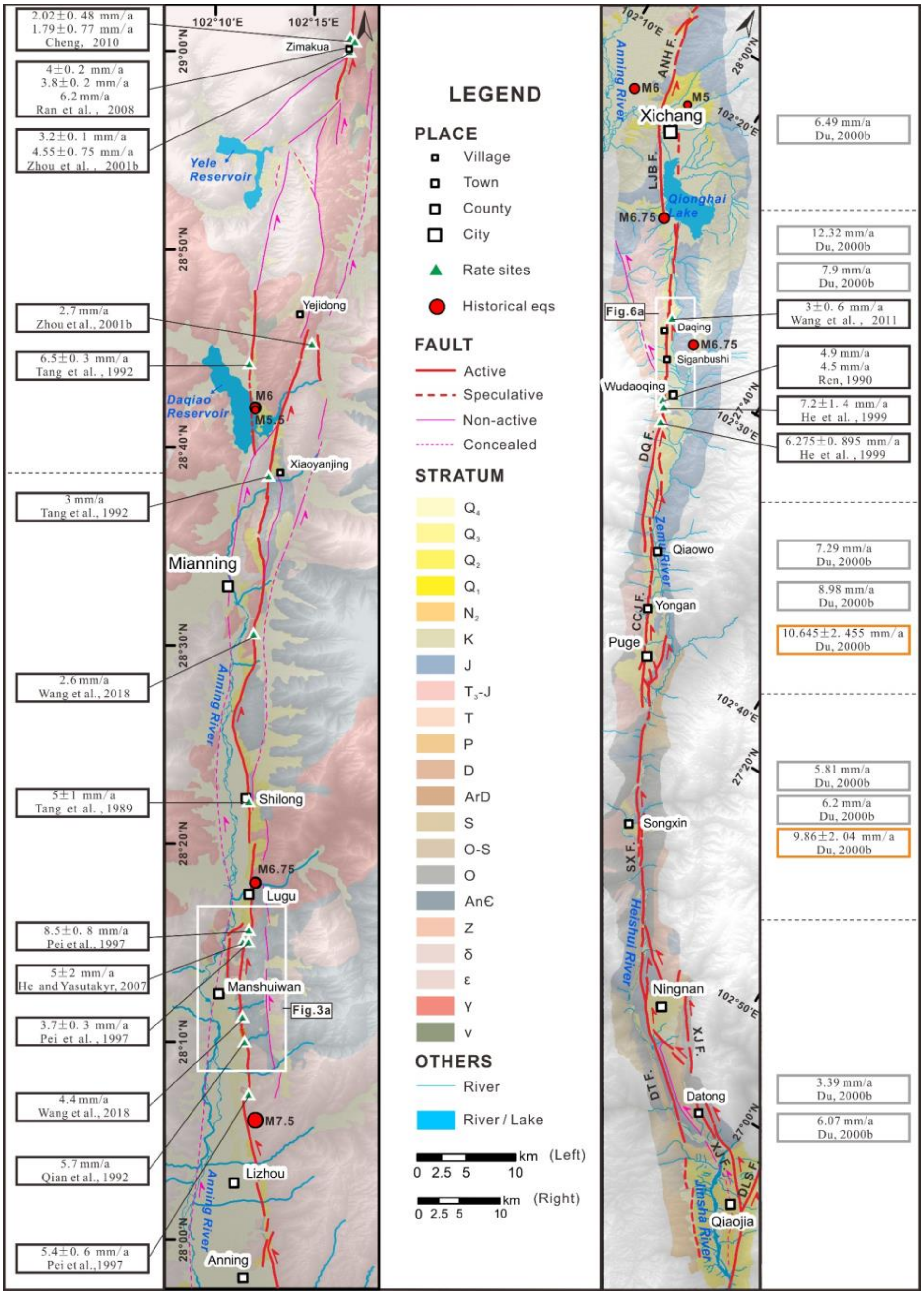

Figure 2. Generalized map of Quaternary deposits along the (a) Anninghe Fault and (b) Zemuhe Fault showing locations of MJG and WDQ sites. The dashed lines in the two boxes on both sides of (a) and (b) separate each segment of the two faults. Black boxes accommodate previous late Quaternary rates at different sites. Gray boxes accommodate previous average late Quaternary rates on each segment, just as that of the orange boxes accommodate previous pre-middle Pleistocene. ANHF.= Anninghe Fault, LJBF.= Lijinbao Fault, DQF.= Daqing Fault, CCJF.= Chechejie Fault, SXF.= Songxin Fault, DTF.= Datong Fault, XJF.= Xiaojiang Fault, DLSF.=Daliangshan Fault.

3 Data and methods

3.1 Mapping and offset identification

To better illustrate fine details at specific sites with subtle morphology, high-resolution hillshades of some displaced features were produced using digital surface models (DSMs) generated using terrestrial laser scanning (TLS). The use of TLS in geomorphology has been driven by the need to produce rapid topographic data that are accurate and precise (Heritage & Large, 2009). It also referred to as terrestrial light detection and ranging (LiDAR) and acquires XYZ coordinates of numerous cloud points on land by emitting laser pulses from the scanner toward the object and measuring the distance between them (Vosselman & Maas, 2010). A point cloud can be converted into a grid digital elevation model (DEM)/Digital Surface Model (DSM) to facilitate topographic mapping and spatial analyses. We collected the cloud point data at two sites in an area of 0.26 km^2 on the Anninghe Fault and an area of 0.4 km^2 on the Zemuhe Fault by TLS in December 2016 (with little vegetation) and generated two DSMs with resolutions of 5 and 10 cm, respectively. Multiple reflectors were used to scan the two sites, which avoided the influence of the scope of the study area and terrain occlusion, and the maximum scanning distance of the scanner always occurs in single reflector scanning. The registration between two cloud points was automatically completed using Stonex Scanner Basic software, and the point clouds were set into the same coordinate system. In Geomagic Studio software, the noise caused by the internal factors of the equipment system and the environmental influence of vegetation, large rocks, and vehicles in the study area was eliminated. The point cloud data of the overlapping area was resampled to eliminate redundant data, reduce the density of point clouds, and improve the reconstruction efficiency of the three-dimensional model. Finally, irregular triangulation was conducted for these discontinuous point cloud data modules to generate the DSM.

The optimal displacements of geomorphic features at the MJG site were gained based on the LaDiCaoz_v2.1 software based on MATLAB (Zielke et al., 2015; Haddon et al., 2016), which were verified in the field. LaDiCaoz—which stands for lateral displacement calculator—was developed to allow quick and easy-to-reproduce measurements of any type of lateral displacement or deflection along strike-slip fault systems in a gridded data set. Offset measurements with LaDiCaoz consist of four steps, namely (1) the manual mapping of the fault and offset channel, (2) an automated offset calculation, (3) back slipping to reconstruct pre-earthquake topography for visual offset measurement assessment, and (4) an automated production of output data (Zielke, 2012). The quality of the offset measurement is determined by a confidence interval, and thus maximum and minimum offsets can be obtained.

The Slope-Enhanced Hillshade of the WDQ site was created in Global Mapper (https://www.bluemarblegeo.com/) from the high-resolution DSM to clear out the gray from low-angle slopes so quaternary map unit colors are not “muddied” by shading (Brown, 2011), and further processed in QGIS (https://www.qgis.org/en/site/) for visualization purposes by blending several layers (Tzvetkov, 2018) and Adobe Illustrator (www.adobe.com/products/illustrator.html) for geomorphic mapping.

3.2 Dating methods

The most common micro geomorphic units in the area are the terraces of grade III, II, and I and the corresponding alluvial or outwash drip fans. The ages of the gravel layer of the terrace or the fan were dated by The Optically Stimulated Luminescence (OSL) or the Radiocarbon (14C) dating method, which approximately represents the abandonment age of the terrace surface or the fan body. In this study, three OSL samples and two 14C samples were dated.

Table 1

Results of OSL dating

No.	Material	Sample location	Burial depth/m	Moisture content/%	Ambient dose rate /(Gy/ka)	Equivalent dose/Gy	Age/ka
SMJG2	Gray white gravel-containing medium-coarse sand	T2	3	6±5	5.7±0.3	320.3±36.1	56.0±6.9
SWDQ2	Gray-yellow clay-containing fine sand	T2	1.2	15±4.5	4.6±0.2	70.5±9.5	15.2±2.1
SWDQ3	Grayish yellow medium fine sand	T2	0.6	15±4.5	4.6±0.2	45.5±7.7	10.0±1.7

The OSL dating method determines the age of materials in sediments, such as quartz and feldspar, since their last exposure to sunlight (Zhang et al., 2015). The sand samples (see **Table 1** for details) were collected using stainless steel tubes (20 cm long and 5 cm in diameter). The tubes were hammered into the sediment, and after complete filling, both ends were immediately sealed with aluminum foil and taped to prevent light leakage and loss of water during transport and storage. The experimental procedure was conducted at the Key Laboratory of Neotectonic Movement and Geohazard, Institute of Geomechanics, Chinese Academy of Geological Sciences. Detailed processing and analytic procedures are reported in a previous study (Chen et al., 2013).

Table 2

Results of 14C dating

Laboratory No.	Sample Code Number	Material	Sample location	Conventional radiocarbon age /BP	2 SIGMA Calendar Calibrated Results / cal BC

Beta-323574	SMJG1	Organic soil	Q_4 Fan	5510±40	4450~4410
Beta-323570	SWDQ1	Carbon chips	T2	16070±70	17470~17000

The Radiocarbon (14C) dating method is the most commonly used technique in active tectonics, enabling to date samples with an age of~5,000–50,000 yr. The organic soil, calcareous sands, and carbon chips were collected at three locations, and detailed sample descriptions and results are shown in **Table 2**. The samples were carried out at Beta Analytic Testing Laboratory, and the radiocarbon dates were calibrated into calendar years with two-sigma errors (95.4% confidence limits) utilizing the OxCal 4.3.2 program with the INTCAL 13 atmospheric curve (Ramsey, 1995; https://c14. arch.ox.ac.uk/oxcal/OxCal.html). All the ages referred to hereafter in this paper are calendar years thus obtained from conventional radiocarbon ages.

4 Investigation and results

4.1 Majiagou (MJG) site

The section of the Anninghe Fault to be discussed here is the west fault of the southern segment of the east branch, which is shown in **Figure 3a**. Developing on the western piedmont of the low mountain, there are varieties of geomorphologic features deflected. Prominently, most of the EW-trending drainages flow from the low mountain showing sinistral nature. The multiphase deluvial fans also have the sign of displacement by the fan scarp or gullies develop on them (**Figure 3b**).

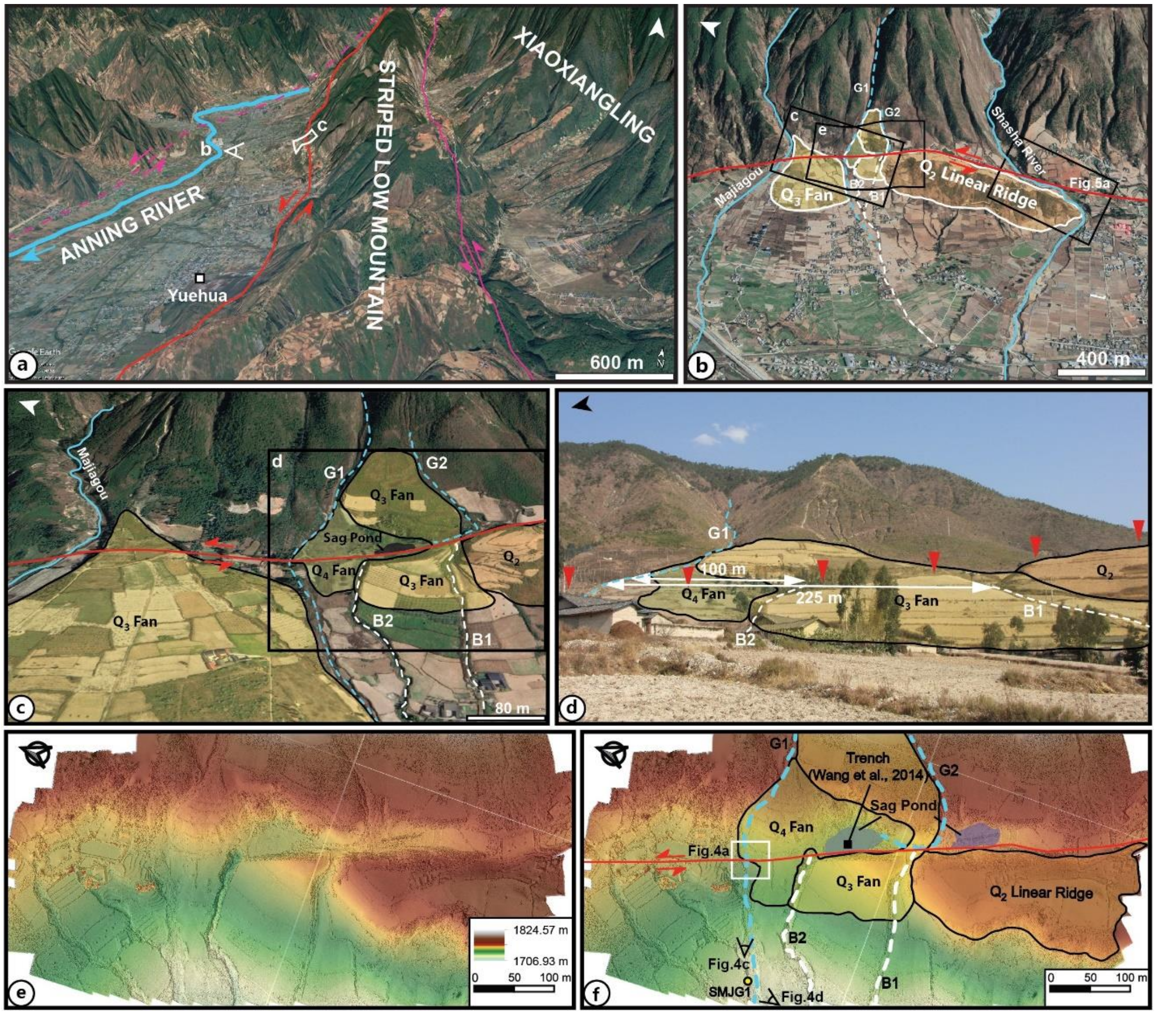

Figure 3. MJG site. (a) Google Earth image of the MJG site area showing the geomorphic feature with the active Anninghe Fault highlighted by the red line and non-active Anninghe Fault with rose-red lines. Rose dashed lines indicates the speculative inactive Anninghe Fault. The blue line highlights the Anning River; (b) Google Earth image of the MJG site and its interpretation, showing the distribution of multi-fans and the displacements. The perspective of it is shown in (a); (c) Google Earth image of the multi-fans and the displacements. The perspective of it is shown in (b); (d) Horizontal offsets (approximately 225/100 m) of the B1 and B2 are visible in the field photo. The trace of Anninghe Fault is highlighted by the red triangles; (e) and (f) DSM (res-5 cm) and its interpretation show the displacement of the Q_4 fan. A solid circle represents collected a sample. The trace of Anninghe Fault is highlighted by the red line. Transparent filled areas indicate the fans. The location can be seen in (b). G1 and G2 represent Modern gully, and B1 and B2 indicate beheaded drainages.

MJG site (N28°10′25″, E102°11′23″) is located between Mianning and Xichang, 42 km and 34 km away from them respectively. The Anninghe Fault passed through these fans with varieties of geomorphological signs preserved, indicating its continuous activity and multi-circle seismic events related to it. Two remarkable beheaded drainages (B1 and B2) were first noticed in Google earth image due to their scales and the sudden break at the knick points (**Figure 3c**). The field observation, especially the gravel layer of the Q_3 Fan carrying them supports that they can be traced to the gully (G1) 225 m and 100 m north of them respectively (**Figure 3d**). Unfortunately, no appropriate ages can be used to constrain the slip rate related to them. A younger fan (Q_4 Fan) cutting the above fan on its north side and spreading south to around B1, was also displaced observed at its north edge (**Figure 3f, Figure 4c**). High-resolution DSM was applied to restore its offset on the LaDiCaoz_v2.1 platform as 23±2 m (**Figure 4b**). This fan's age has a high-confidence with two means to constrain. We sampled at the north scarp of the G1 (sample: SMJG1=14C: 5510±40 a BP, Organic soil, about 2 m below the surface), which represents the age of another Q_4 Fan to the north of G1 (**Figure 4e**). The thickness of the Q_4 Fan (1~2 m) above lower than this fan scarp (2~3 m, **Figure 4d**) indicating a younger age of it, which considers the same tectonic background and similar origin. The bottom age of a sag pond on the studied Q_4 Fan revealed through the combined trench at the east side of the Q_2 linear ridge was 3100±30 a BP (Wang et al., 2014) (**Figure 3f**). This sag pond and another one south of it are thought to the product of the activity of the Anninghe Fault under the block of the above linear ridge, which must occur after the Q_4 Fan formed. Adopting the lower age limit, we affirm the maximum slip rate at this site as 7.4±0.7 mm/a since the Late Holocene. Incidentally and notably, the combined trench excavated by Wang et al. (2014) recognized five paleoseismology events, instructing the offset of the Q_4 Fan is corresponds to the coseismic surface displacement of five paleoearthquakes. Taking the hypothesis of the stable activity of the Anninghe Fault in Late Quaternary, we believe that the coseismic surface displacement is about 4.6 m per earthquake. Therefrom, the magnitudes of these paleoearthquakes can be calculated to be Mw7.3 according to the functional relationship between the maximum coseismic displacement and the moment magnitude of Wells & Coppersmith (1994). The magnitudes of four historical earthquakes associated with three paleoseismology events (Event1: one of the M $7^{1}/_{2}$ 1850 AD and M $6^{3}/_{4}$ 1952 AD earthquake, Event2: the M $7^{1}/_{2}$ 1536 AD earthquake, and Event4: the M 7 814 AD earthquake) further prove the reliability of our research. The deflection of the Shasha River, south of MJG, was influenced by the above linear ridge, and the T2/T3 terrace riser of it has a deflection of 380±10 m on the side offset away from the River course, measuring on the Google Earth (**Figure 5a, 5b**). On this consideration, the "Upper terrace model" is more perfect to use here to calculate the slip rate (Cowgill, 2007; Zhang et al., 2008). However, the abandonment age of the T2 surface was tested instead of that of the T3 surface, which is 56.0±6.9 ka (sample: SMJG2, Gray white gravel-containing medium-coarse sand, 4 m below the T2 surface). We can only make the highest constrain of the slip rate as 6.9±1 mm/a (**Table 3**).

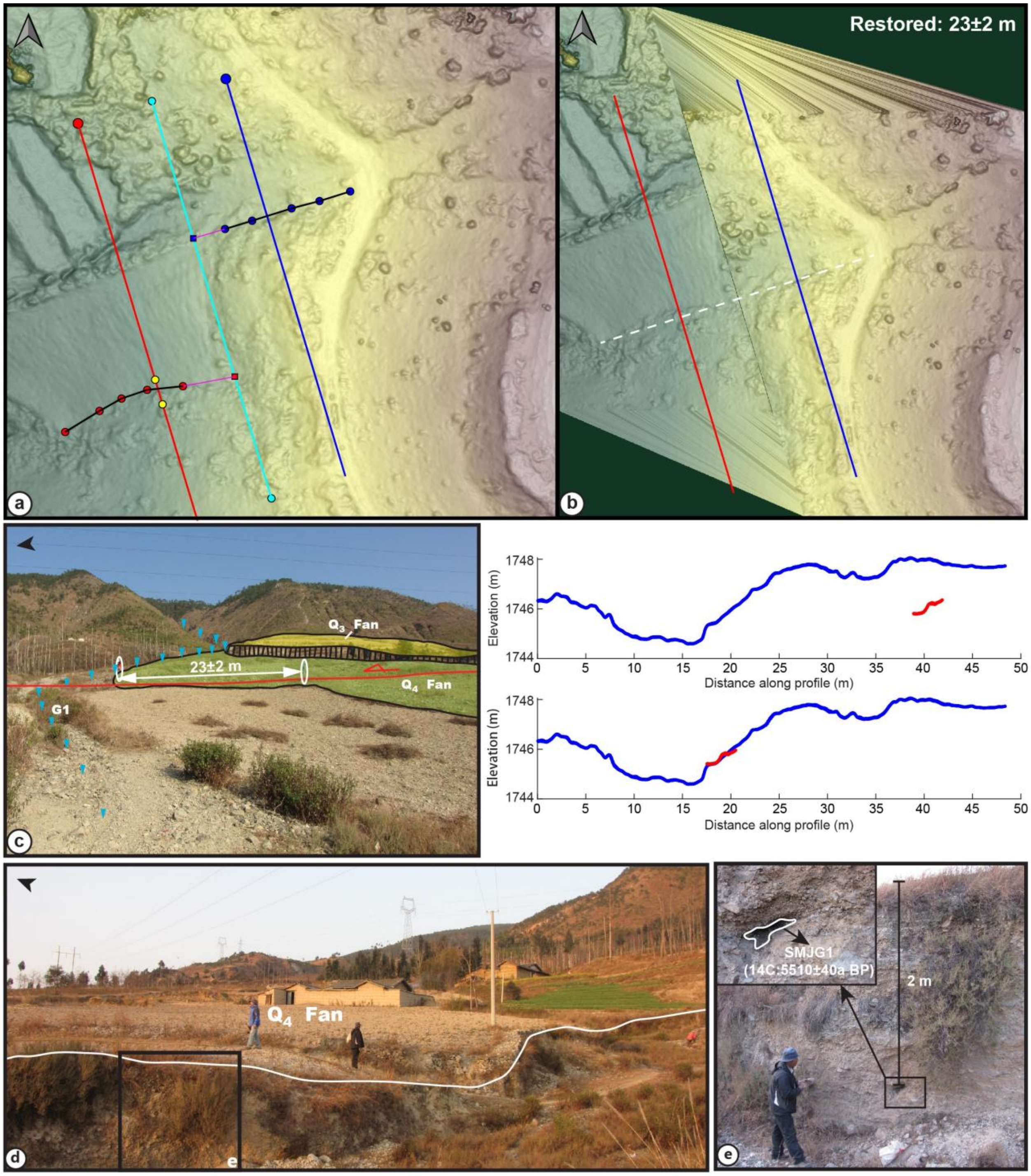

Figure 4. MJG site. (a) and (b) DSM (res-5 cm) shows the restored left-lateral displaced fan edge of the Q_4 fan with 23±2 m offset. The range is shown in Figure 3f. The topographic profile (middle right) shows the left-lateral displacement. The offset was measured using LaDiCaoz_v2.1 (see text). (c) Field photo shows the displaced characteristics of the Q_4 fan. The overview of this area is shown in Figure 3f. (d) Field photo illustrates the characteristics of the latest fan originating from Majiagou, which is separated from the studied Q_4 fan by G1. The overview of this area is illustrated in Figure 3f. (e) The north scarp of the G1 where the sample

SMJG1 was collected. The inset photo shows sample SMJG1 (14C: 5510±40 a BP) at a height of 2 m from the ground.

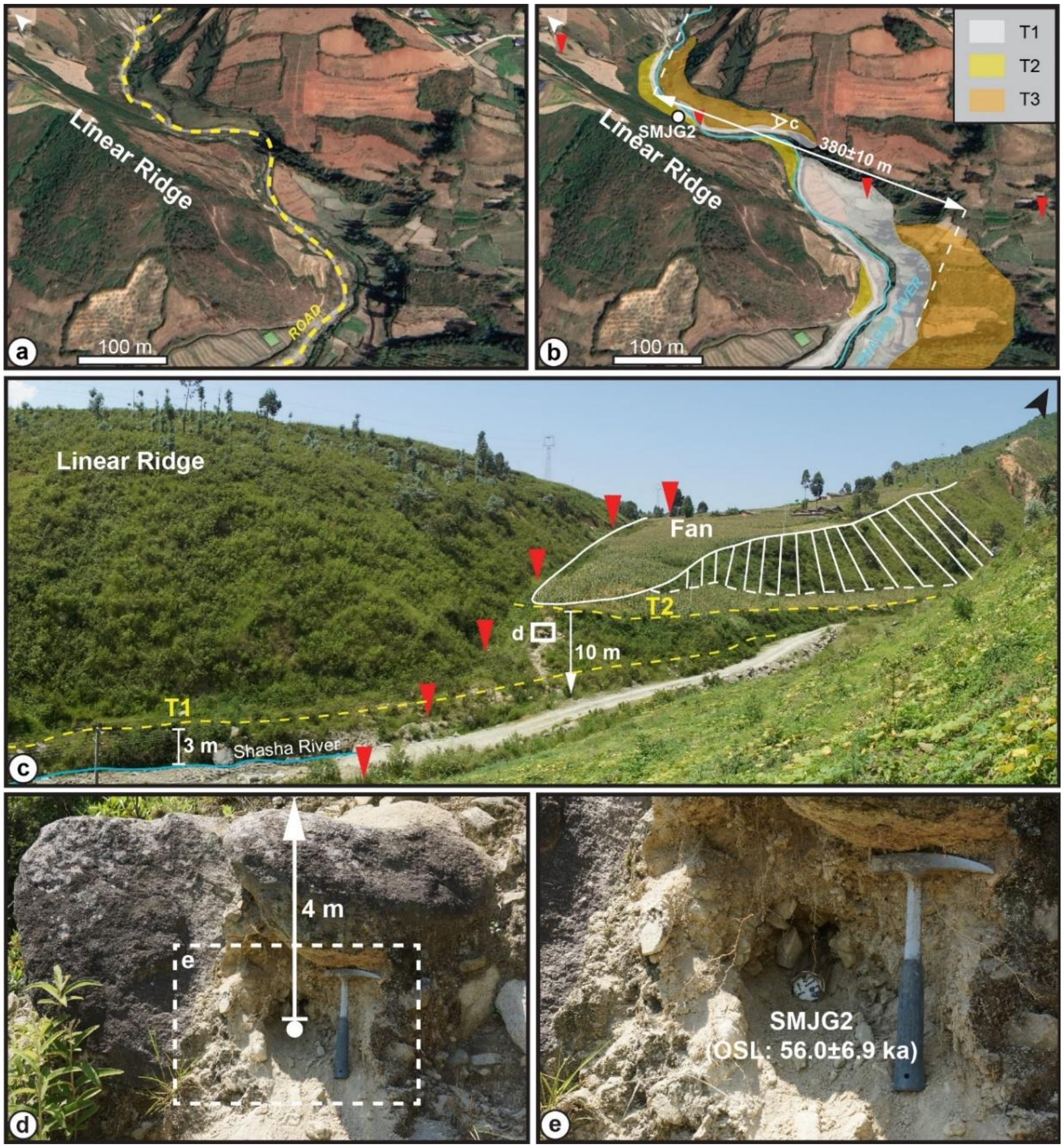

Figure 5. Shasha River site, approximately 1 km south of MJG site. (a) and (b) Google Earth images of the Shasha River site and its interpretation, showing the displacements of multi-risers of the Shasha River. The offset of 380±10 m of the T2/T3 riser is marked with a white line. Solid circles represent collected sample. The location of it is shown in Figure 3b. (c) Field photo illustrates the character of the near range landform. Red arrowheads indicate the active fault trace. T1 and T2 are sketched with dashed yellow lines, with their height from Shasha River measured to 3 and 10 m. A fan developing on the T2 is also illustrated. Perspectives of photograph is located in (b). (d) and (e) Field photos of the profile and location of sample SMJG2 (OSL: 56.0±6.9 ka). The white arrow pointing up in (d) represents the height of the sample from the ground.

4.2 Wudaoqing (WDQ) site

Siganbushi is the center and the pivot axis of the Daqing Fault, controlling the landform on both sides of the fault, which presents characteristics of the four-quadrant distribution (Feng & Du, 2000). The east side of the north and south sections of the fault are the Daqingliangzi Uplift and Wudaoqing Basin, respectively; the west side of the north and south section are the West Branch Valley of the Zemu River and the alluvial platform of the eastern piedmont of Luoji Mountain, respectively (**Figure 6a**). On the alluvial platform of the eastern piedmont of Luoji Mountain, the WDQ site (N27°37′50″, E102°24′10″) is located between Xichang City and Puge County at 30 km from each region. As the origin of two terraces (T3, T2), which only formed at the south side of the mountain mouth and deflected afterward, Baijiawanzi was curved in an "elbow" shape (**Figure 6b**). On the north side, the bedrock of the Luoji Mountain connects to Baijiawanzi directly, with some sediments of younger eroded terraces separating them locally. With the incising of Baijiawanzi, T3 ceased sediment deposition at approximately 53.53±2.62 ka, which was constrained by a Thermoluminescence (TL) sample (sample: SWDQ4) of silty fine sand taken from its uppermost gravel layer (Yu, 2010, **Figure 6c**). In the process of deflection of T3, T2 had started to deposit on it before 25.51±2.69 ka (sample: SWDQ5). The age was dated on a TL sample of a 10–20 cm thick sand lens, which was found at the bottom of the scarp 3 m above the Baijiawanzi (Yu, 2010, **Figure 6c**). Until approximately 16070±70 a BP (sample: SWDQ1) or 15.2±2.1 ka (sample: SWDQ2) on the upstream and 10.0±1.7 ka (sample: SWDQ3) on the downstream of T2 with the Daqing Fault as the bound, the surface of the T2 was abandoned under the incision of the Baijiawanzi, with a 15 m high scarp forming on the upstream and 10 m high scarp on the downstream (**Figure 6c, 6f**). The significant difference in scarp dating indicates the characteristic forming diachroneity of the scarps, owing to the different termination time of fluvial erosion (Cowgill, 2007) or because of the younger sediment on the downstream side, which should be excluded from slip rate calculation. The deflection of the T2 scarp was measured to be 180±5 m on the slope-enhanced hillshade from the TLS data (**Figure 6d, 6e**). Considering that deflection is on the side offset from the River course, the "upper terrace model" is suitable to calculate the slip rate (Cowgill, 2007; Zhang et al., 2008). The age of the 14C sample on the upstream was used to determine the slip rate of the Daqing Fault to 11.2±0.4 mm/a, and the age of the OSL sample was used as a reference.

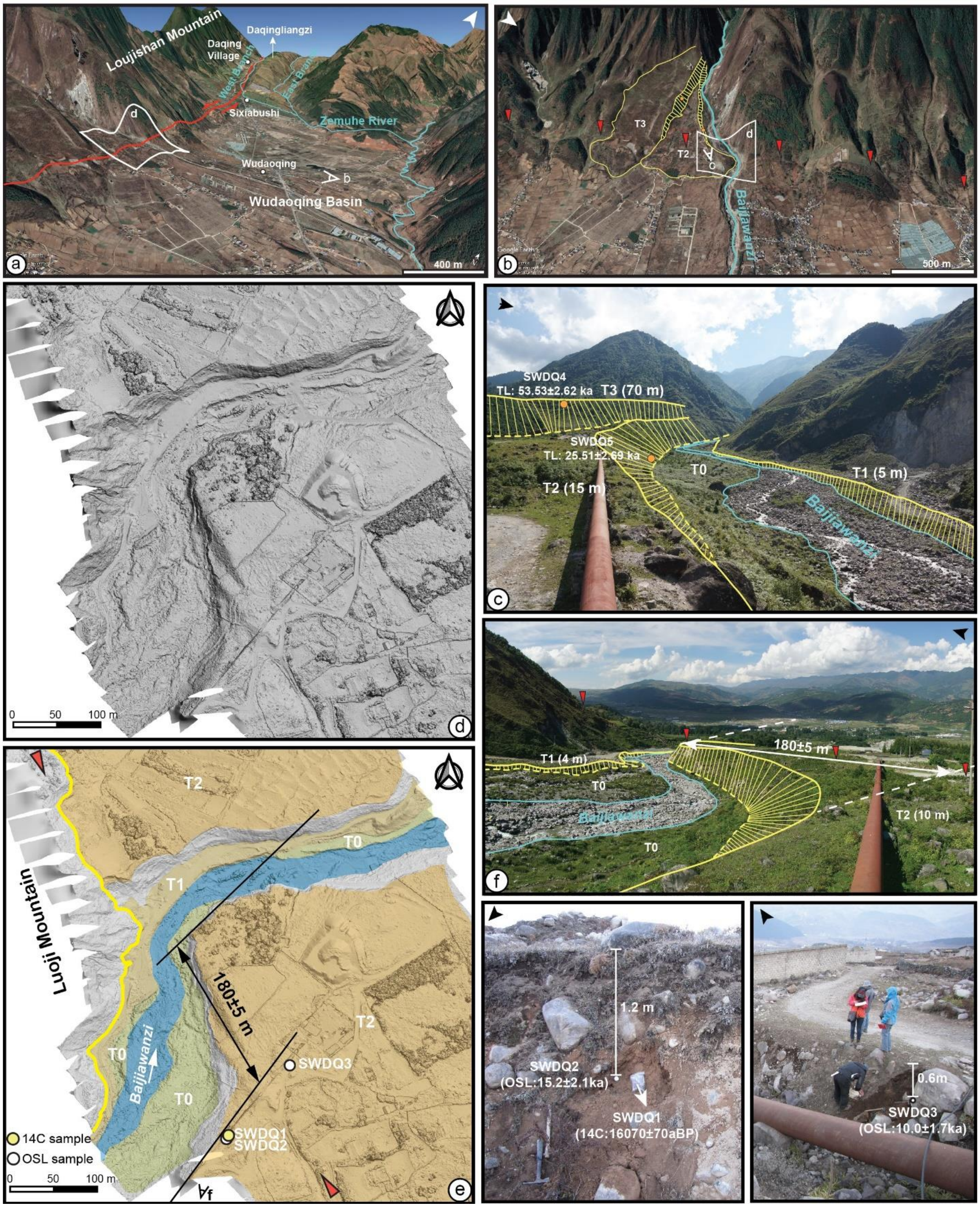

Figure 6. WDQ site. (a) and (b) Google Earth images showing the landforms from far and proximate perspectives, respectively; red line and red arrows mark the Zemuhe Fault trace in (a) and (b); (c) Field photo of the relationship between the two terraces and Baijiawanzi stream. The values in brackets indicate the heights of the terrace surfaces above the river; (d) and (e)

Displaced terrace of the "elbow" shaped Baijiawanzi mapped in the slope-enhanced hillshade. Red arrows indicate the active fault trace. Yellow line indicates the piedmont of the Luoji Mountain. The solid circles indicate sample sites; (f) Field photo shows the displacement of T2 scarp, with red arrows marking the Zemuhe Fault trace. The values in brackets have the same meaning as the ones in (c). Two field photographs in the lower right corner show the character and locations of samples SWDQ1 (14C: 16070±70 a BP), SWDQ2 (OSL: 15.2±2.1 ka), and SWDQ3 (OSL: 10.0±1.7 ka). Their depth from the ground are marked with white lines. Their locations are indicated in (e). The arrows at the upper-right/left point north.

Table 3

Results of fault slip rate estimates along the Anninghe–Zemuhe Fault Zone

Fault	Site	Geomorphic marker	Slip rate (mm/a)	Offset (m)	Age	Age source
Southern segment of Anninghe Fault	MJG	Beheaded drainage1	-	225	-	-
Southern segment of Anninghe Fault	MJG	Beheaded drainage2	-	100	-	-
Southern segment of Anninghe Fault	MJG	northern edge of Q_4 fan	7.4±0.7	23±2	3100±30 a BP	Wang et al., 2014
Southern segment of Anninghe Fault	South of MJG	T2/T3 riser of Shasha River	6.9±1	380±10	56.0±6.9 ka	This paper
Daqing Fault of the Zemuhe Fault	WDQ	T2 Scarp	11.2±0.4	180±5	16070±70 a BP	This paper

5 Discussion

5.1 The late Quaternary strike-slip rates of the XXFS along-strike

Slip rates on the XXFS have been estimated at various time scales along its strike (**Figure 7**). The late Quaternary strike-slip rate will be discussed particularly.

The sinistral strike-slip of the Xianshuihe Fault may initiate approximately 10 Ma ago. Its trace shows a significant difference with Bamei as the center, which is uniform to the north and disperses to the south. Passing southward after Kangding, the trace becomes uniform again. The average Late Quaternary strike-slip rate of the northwestern segment is 12.79 mm/a (Qian et al., 1988; Wen et al., 1989; Deng, 1989; Li et al., 1997; Xiong et al., 2010; Chen et al., 2016; Zhang et al., 2016). The strike-slip rates of the three branches on the middle segment ranges from 0.6 to 10.7 mm/a (Wen et al., 1989; Allen et al., 1991; Li et al., 1997; Zhou et al., 2001a; Chen et al., 2016; Zhang et al., 2016; Yan & Lin, 2017; Bai et al., 2018), but their sum is comparable to that of the northwestern segment, which is 12.23 mm/a. The slip rate on the southeastern segment reveals a notable decreasing trend, and a one-third reduction was observed (Deng, 1989; Li et al., 1997; Zhou et al., 2001a; Chen et al., 2016; Zhang et al., 2016), which is consistent with the absence of historical earthquakes greater than M6 at this section (**Figure 1**). It is supposed that the southeastward thrust of the perpendical Longmenshan Fault weaken the lateral slip of the southern segment of Xianshuihe Fault. We also collected activity data for the whole fault before the middle-Pleistocene (Roger et al., 1995; Wang et al., 2012; Yan & Lin, 2015; Zhang et al., 2017) and during the modern period (Xu et al., 2003; Qiao et al., 2004; Shen et al., 2005; Tang et al., 2005a, 2005b, 2007; Gan et al., 2007; Peng et al., 2007; Peng et al., 2007; Wang et al., 2008; Wang et al., 2009; Loveless & Meade, 2011; Cheng et al., 2011; Zhang, 2013; Jiang et al., 2015; Zheng et al., 2017; Wang et al., 2017a; Wang et al., 2017b), which is averaged to 5.87 and 11.05 mm/a, respectively. Thus, we concluded that the activity of the Xianshuihe Fault not only changes spatially, reducing from north to south, but also changes temporally, accelerating from the pre-middle Pleistocene to the late Quaternary until the present.

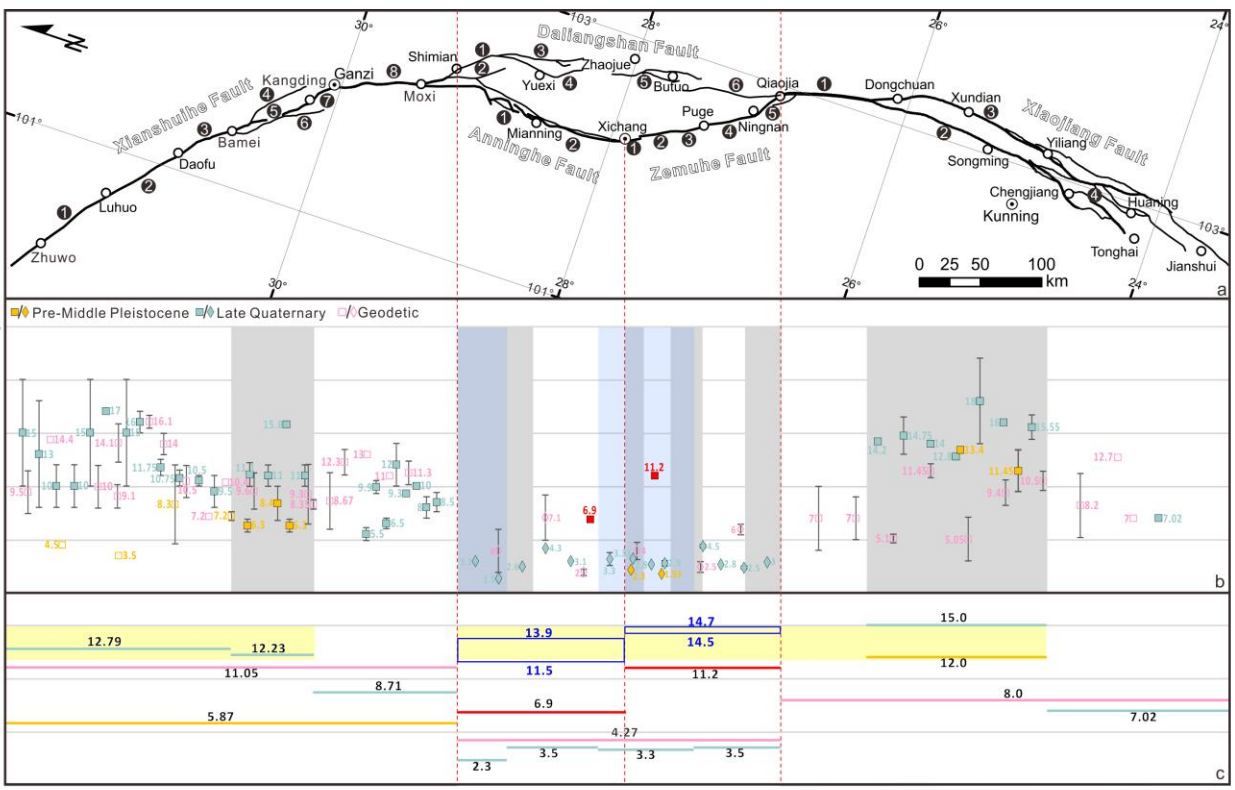

Figure 7. (a) Spatial distribution of each fault of the XXFS: Xianshuihe Fault consists of three segments with eight faults in total. ① Luhuo Fault, ② Daofu Fault, and ③ Qianning Fault belong to the Northwestern segment. ④ Yalaha, ⑤ Selaha, and ⑥ Zheduotang faults form the middle segment. Thus, the slip rates marked in these sections in (b) is the sum of the three slip rates. The southeastern segment consists of the ⑦ Kangding Fault and ⑧ Moxi Fault. Anninghe Fault is separated by Mianning, so two segments are noted. For the Zemuhe Fault, the five numbers refer to ① Lijinbao, ② Daqing, ③ Chechejie, ④ Songxin, and ⑤ Datong faults.

Xiaojiang Fault is divided into three segments, and the middle segment consists of two branches, so the slip rates labelled in (b) is the sum of them. Daliangshan Fault contains six secondary faults (① Zhuma Fault, ② Gongyihai Fault, ③ Puxiong Fault, ④ Yuexi Fault, ⑤ Butuo Fault, and ⑥ Jiaojihe Fault), and the slip rates of only four (①, ③, ⑤, and ⑥) are shown in (b) due to the limited data; (b) strike-slip rates along strike of the XXFS at different time scales (represented by various colors, with orange, ocean green, and pink referring to the slip rate of Pre-Late Pleistocene, Late Quaternary, and Geodetics, respectively), see the corresponding detailed slip rate statistics in the **Table S1**. For the middle section, the slip rates of Daliangshan Fault and Anninghe Fault / Zemuhe Fault are indicated with diamond labels and square labels, respectively. Red square labels refer to the data obtained in this paper. Segments of each fault are distinguished with gray bands for the faults except Daliangshan Fault, which is segmented with blue bands; (c) Average strike-slip rates along strike of the XXFS at different time scales (labeled with various colors, with orange, ocean green, and pink referring to the slip rate of Pre-Late Pleistocene, Late Quaternary, and Geodetics, respectively). The red lines refer to the average results of the Anninghe Fault and Zemuhe Fault in this paper, and the dark blue hollow rectangle indicates the total slip rate of Anninghe Fault/Zemuhe Fault and Daliangshan Fault. The slip rate of the XXFS is constrained from ~12 mm/a (north) to ~15 mm/a (south), with the southern segment of Xianshuihe Fault ruled out, illustrated with a yellow band.

The strike-slip rates of the northern segment and the two branches of the middle segment of the Xiaojiang Fault are comparable, with both being higher than that on any of the small faults in the southern segment. The pre-middle Pleistocene slip rate of the middle segment is ~12 mm/a (Song et al., 1998). The late Quaternary slip rate of the northern segment is suggested to be about 12 mm/a according our own unpublished data revealed by the same methods and data as this paper. The sum of the late Quaternary slip rate of the two branches of the middle segment is ~15 mm/a (Chen & Li, 1988; Song et al., 1998; Geology Institute of China Seismological Bureau and Seismological Bureau of Yunnan Province, 1990; He et al., 2002; Shen et al., 2003; He & Oguchi, 2008). That of the southern segment was measured to be 7.02 mm/a by Han et al. (2017). Comprehensively considering the results of previous studies, the modern slip rate of the whole fault deduced from GPS data ranges from 5.05 to 12.7 mm/a, which is averaged to ~8 mm/a (Shen et al., 2005; Wang et al., 2008; Wen et al., 2011; Loveless & Meade, 2011; Cheng et al., 2011; Shi et al., 2012; Wei et al., 2012a; Liu et al., 2015; Wang et al., 2017b; Zheng et al., 2017). The lower rate might be negatively impacted by the broad southern segment where the fault-perpendicular GPS profiles did not cover the entire fault, thus ignoring some deformation. In general, the section north of Yiliang of the Xiaojiang Fault has maintained a high activity of 12–15 mm/a since its formation. The section to the south of Yiliang, referring to the southern segment of Xiaojiang Fault, decomposes into numerous branches with low and difficult-obtained slip rates in a broad belt. The major fault of the Xiaojiang Fault likely does not pass through the NW right-lateral strike-slip Red River Fault Zone, but the strain rate revealed by the GPS indicates a level comparable to that of the north side of the Red River Fault Zone. Beyond strike-slip faulting, the mechanism by which the strain rate is absorbed should be researched further.

In this study, the two late Quaternary slip rates of the Anninghe Fault are averaged to 6.9 ± 0.6 mm/a, which is higher than the previous result. Our result (11.2 ± 0.4 mm/a) on the Zemuhe Fault is also higher than the previous result. Indeed, a slip rate deficit definitely exists at the Anninghe–Zemuhe section relative to the XXFS, most notably on the Anninghe Fault. This implies that a deformation transition occurs in this section in the process of the movement of the SE margin of the Tibetan Plateau. It has been previously suggested that the rate deficit is transferred into crustal across-strike shortening (Xu et al., 2003), which is inconsistent with the strain rate field obtained from GPS measurements (Gan et al., 2007). Alternatively, the deformation is thought to be spatially separated (or "partitioned") into other parallel strike-slip faults (Xu & Stamps, 2019), and it is supposed that the Daliangshan Fault 50 km east of the Anninghe–Zemuhe Fault Zone contributes to the southeastward motion of the SE margin of the Tibetan Plateau (He et al., 2006, 2008).

The Daliangshan Fault contains six individual faults: the Zhuma, Gongyihai, Puxiong, Yuexi, Butuo, and Jiaojihe faults from north to south. The Late Quaternary strike-slip rates of four faults (Zhuma Fault, Puxiong Fault, Butuo Fault, and Jiaojihe Fault) were calculated to be 2.3±0.8, 3.5±0.9, 3.3±0.6, and 3.5±1.1 mm/a (**Figure 7**, Shen et al., 2000; Zhou et al., 2003; Chen, 2006; He et al., 2008; Wei et al., 2012b; Sun et al., 2015). A higher value of 4.27 mm/a for the entire fault was obtained by GPS observation (Shen et al., 2005; Wang et al., 2008; Loveless & Meade, 2011; Cheng et al., 2011; Zhang, 2013; Wang et al., 2017b). It has been proven that off-fault deformation occurs in the stretching area, accounting for the total deformation monitored with geodetic measurements (Karabacak et al., 2020). In the extension Anninghe–Zemuhe section area (Gan et al., 2007), the GPS result of the fault belt is larger than the geological results obtained for individual faults.

The slip rates of the three faults (Xianshuihe Fault, Anninghe–Zemuhe Fault Zone, and Xiaojiang Fault) obtained from available geological data are ~12, 6.9–11.2, and 12–15 mm/a, respectively. The Zhuma Fault and Gongyihai Fault roughly spatially correspond with the northern segment of the Anninghe Fault, just as the Puxiong Fault and Yuexi Fault spatially correspond with the southern segment of the Anninghe Fault. Therefore, the slip rate of the Daliangshan Fault corresponding to the section of Anninghe Fault is in the range of 4.6–7.0 mm/a, which indicates a slip rate of 11.5–13.9 mm/a of the Anninghe-Daliangshan section. The obvious slip rate deficit on the Zemuhe section is compensated by the slip rate of 3.3–3.5 mm/a of the Butuo Fault and Jiaojihe Fault. Therefore, the sum of the slip rates of the Zemuhe Fault and Daliangshan Fault is between 14.5 and 14.7 mm/a. Moreover, the GPS velocity field across the entire Daliangshan area also shows that the sum of the velocities of Anninghe Fault and Daliangshan Fault is equivalent to that obtained by the velocity profile across the Xianshuihe Fault (Zhang, 2013; Li et al., 2020). Therefore, the left-lateral strike-slip of the XXFS north of Yiliang has an approximately constant slip rate of 12–15 mm/a along-strike, with the southern segment of Xianshuihe Fault ruled out, exhibiting a slight increase southward.

In addition, the maximum offsets of geological or geomorphological markers along Xianshuihe Fault, Anninghe–Zemuhe Fault Zone, and Xiaojiang Fault show differences of 60, 47–53, and 48–63 km, respectively (Wang et al., 1998). The maximum offset is 10–15 km along the different faults of the Daliangshan Fault (Shen et al., 2000; Pan, 2005), covering the offset deficit on the Anninghe–Zemuhe Fault Zone relative to the Xianshuihe Fault and Xiaojiang Fault. In summary, the existence of the Daliangshan Fault makes the XXFS have a complete arc-shaped structure geometrically, which conforms to the self-smoothing characteristics of the fault system to improve sliding (Zhang, 2013). Together with the Anninghe–Zemuhe Fault Zone, the Daliangshan Fault consists of the boundary of the SE margin of the Tibetan Plateau as a whole in the Anninghe–Zemuhe section.

5.2 Clockwise block rotation of the SE margin of the Tibetan Plateau

It is definite that strike-slip on the faults in the SE margin of the Tibetan Plateau and the rotation of this region itself accommodate the eastward extrusion of the Tibet (Molnar & Lyon-Caen, 1989; Xu et al., 2003). Notably, strike-slip on the XXFS takes up a large amount of the extrusion strain, with a little component absorbed by other left-lateral strike-slip faults within the SE margin of the Tibetan Plateau, such as Wanding, Nantinghe, Litang, and Lijiang-Xiaojinhe faults. The effect of the right-lateral faults inner should be excluded due to their weak activity. For example, the slip rate of the Red River Fault is lower almost one order of magnitude than that of the XXFS (Shi et al., 2018). The remaining extrusion strain accommodated by rotation of the SE margin of the Tibetan Plateau is disputed on whether the strain is absorbed by the sub-block rotation or the block rotation (Molnar & Lyon-Caen, 1989; Xu et al., 2003). The sub-block rotaion model emphasizes that the block is divided into several sub-blocks by a series of sub-parallel strike-slip faults, which move apart and rotate accompanying with the lateral shear of the boundary faults that bounded the block (**Figure 8a**). Here those sub-parallel strike-slip faults have the same slip sense and it is the displacement on the boundary faults that controls the sub-block rotation (Xu et al., 2003; McKenzie & Jackson, 1986). Considering the weak activity of the Red River Fault, it is suspected that the sub-block rotation model not applicable in this region. It is suggested that the block rotation model is probably more applicable in this region (**Figure 8b**). In detail, under the constraint of the curved XXFS which concaves toward the west, there must be a rotation of the material on its west side with respect to the other side. It is concluded that the SE margin of the Tibetan Plateau rotates around the EHS under the constraint of the XXFS. Particularly, the unified rotation allows local strain difference around those inner faults.

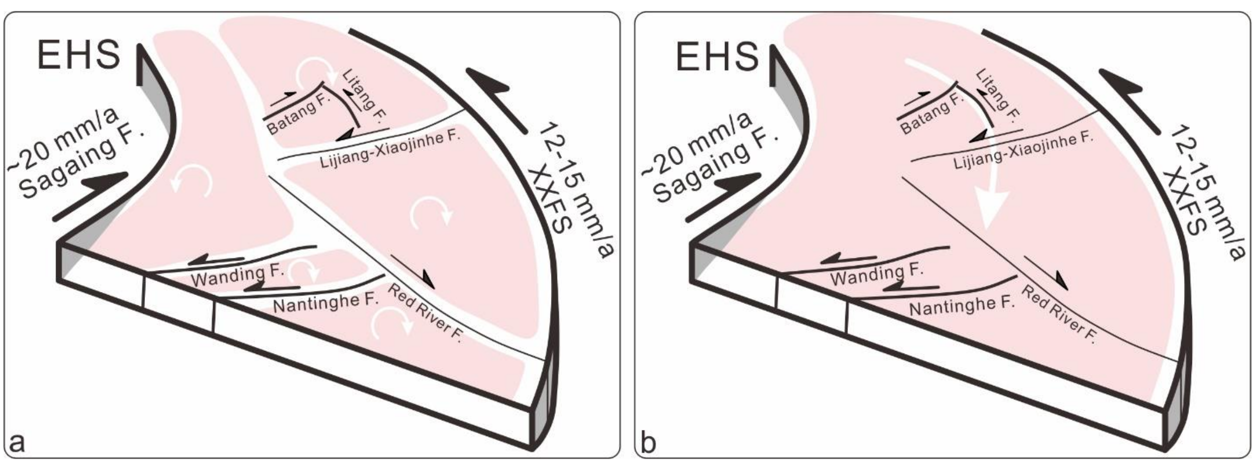

Figure 8. Rotation models of the SE margin of the Tibetan Plateau. (a) Sub-blocks rotation model (modified from Shi et al., 2017); (b) block rotation model.

6 Conclusion

In this study, we investigated two sites showing horizontal offsets along the Anninghe Fault and Zemuhe Fault to evaluate their late Quaternary slip rates. By measuring the offsets of the Q_4 Fan edge at the MJG site and the T2/T3 riser to its south, and that of a terrace scarp at the WDQ site, and dating their surfaces using OSL and 14C, we determined reliable late Quaternary slip rates of 6.9±0.6 mm/a along the Anninghe Fault and of 11.2±0.4 mm/a along the Zemuhe Fault. The Anninghe–Zemuhe section is a transition area where the slip rate decreases, and the maximum offset is less than that of Xianshuihe Fault and Xiaojiang Fault. According to the investigation of the Daliangshan Fault on the same aspects as the Anninghe Fault and Zemuhe Fault, we found that the Daliangshan Fault compensates for the deficient slip rate and balances the maximum offset on each segment of the XXFS, forming a part of the XXFS in the Anninghe–Zemuhe section. We further reanalyzed the slip rate of each section of the XXFS along strike by conducting a large of rate statistics. It is concluded that the slip rate of the XXFS north of Yiliang is in a narrow range of 12–15 mm/a, exhibiting a slight increase southward. Combined with the analysis of the relationship between the active faults and block rotation, we proposed that the uniform high-speed strike-slip along the Xianshuihe–Xiaojiang Fault System largely constrains the clockwise rotation of the SE margin of the Tibetan Plateau.

Acknowledgments

The authors are grateful to the editor and two anonymous reviewers for their thorough and constructive reviews, which greatly improved the quality of this manuscript. The first author also thanks the China Scholarship Council (CSC) for the scholarship and financial support. This research has been funded by the financial grants from the National Natural Scientific Foundation of China (Grant Number: U2002211) and the China Geology Survey Projects (Grant Numbers: 12120114002101, DD20160268).

The slip rates along the Xianshuihe-Xiaojiang Fault System solicited from literatures, which are listed in **Table S1**.

References

Allen, C.R., Luo, Z.L., Qian, H., Wen, X.Z., Zhou, H.W., Huang, W.S., 1991. Field study of a highly active fault zone: The Xianshuihe fault of southwestern China. Geological Society of America Bulletin, 103, 1178–1199.

Armijo, R., Tapponnier, P., Han, T.L., 1989. Late Cenozoic right-lateral strike-slip faulting in southern Tibet. J. Geophys. Res., 94(B3), 2787–2838.

Avouac, J.P., & Tapponnier, P., 1993. Kinematic model of active deformation in central Asia. Geophys. Res. Lett., 20(10), 895–898.

Bai, M.K., Chevalier, M.L., Pan, J.W., Replumaz, A., Leloup, P.H., Métois, M., Li, H.B., 2018. Southeastward increase of the late Quaternary slip-rate of the Xianshuihe fault, eastern Tibet. Geodynamic and seismic hazard implications. Earth and Planetary Science Letters, 485, 19–31. https://doi.org/10.1016/j.epsl.2017.12.045.

Brown, D.K., 2011. Creating Slope-Enhanced Shaded Relief Using Global Mapper.

Chen, G.H., 2006. Structural transformation and stain partitioning along the northeast boundary belt of the Sichuan-Yunnan Block. Beijing: Institute of Geology, China Earthquake Administrator, PhD thesis (in Chinese with English abstract).

Chen, G.H., Xu, X.W., Wen, X.Z., Chen, Y.G., 2016. Late Quaternary Slip-rates and Slip Partitioning on the Southeastern Xianshuihe Fault System, Eastern Tibetan Plateau. Acta Geologica Sinica (English Edition), 90(2), 537–554.

Chen, R., & Li, P., 1988. Slip rates and earthquake recurrence interval of the western branch of the Xiaojiang Fault Zone. Seismology and Geology, 10(2), 1–12 (in Chinese with English abstract).

Chen, Y.W., Li, S.H., Sun, J.M., Fu, B.H., 2013. OSL dating of offset streams across the Altyn Tagh Fault: Channel deflection, loess deposition and implication for the slip rate. Tectonophysics, 594, 182–194.

Cheng, J., Liu, J., Gan, W.J., Yu, H.Z., Li, G., 2011. Characteristics of strong earthquake evolution around the eastern boundary faults of the Sichuan-Yunnan rhombic block. Science China Earth Sciences, 54(11), 1716–1729 (in Chinese with English Abstract).

Cheng, J.W., 2010. A study on the Stratigraghy and Tectonic Activity during the Late Quaternary of the Anning River Fault in western Sichuan Province of China. Beijing, Institute of Geology, China Earthquake Administration, PhD Thesis (in Chinese with English Abstract).

Chevalier, M.L., Leloup, P.H., Replumaz, A., Pan, J.W., Métois, M., Li, H.B., 2017. Temporally constant slip rate along the Ganzi fault, NW Xianshuihe fault system, eastern Tibet. Geological Society of America Bulletin, 130(3), doi: 10.1130/B31691.1.

Clark, M.K., & Royden, L.H., 2000. Topographic ooze: building the eastern margin of Tibet by lower crustal flow. Geology, 28 (8), 703–706.

Cowgill, E., 2007. Impact of riser reconstructions on estimation of secular variation in rates of strike–slip faulting: Revisiting the Cherchen River site along the Altyn Tagh Fault, NW China. Earth and Planetary Science Letters, 254(3–4), 239–255.

Deng, T.G., 1989. Xianshuihe Active Fault Zone. Chengdu: Sichuan Science Press (in Chinese).

Du, P.S., 2000a. Evolution Histories and Deformarion Mechanism about Active Fault of Zemuhe. Earthquake Research in Sichuan, 1–2, 65–79 (in Chinese with English abstract).

Du, P.S., 2000b. Slip displacement and its rate about Zemuhe Faults. Earthquake Research in Sichuan, 1–2, 49–64 (in Chinese with English abstract).

England, P., & Houseman, G., 1986. Finite strain calculations of continental deformation: 2. Comparison with the India-Asia collision zone. Journal of Geophysical Research, 91(B3), 3664–3676. https://doi.org/10.1029/JB091iB03p03664.

England, P., & Molnar, P., 1997. Active deformation of Asia: From kinematics to dynamics. Science, 278(5338), 647–650.

Feng, Y.B., & Du, P.S., 2000. Geologic Tectonic and Earthquake Preparation Conditions about 1850 Xichang Earthquake. Earthquake Research in Sichuan, 1–2, 97–101(in Chinese with English abstract).

Gan, W.J., Zhang, P.Z., Shen, Z.K., Niu, Z.J., Wang, M., Wan, Y.G., Zhou, D.M., Cheng, J., 2007. Present-day crustal motion within the Tibetan Plateau inferred from GPS measurements. Journal of Geophysical Research, v. 112, p. B08416, doi: 10.1029/2005JB004120.

Geology Institute of China Seismological Bureau and Seismological Bureau of Yunnan Province, 1990. Active faults in northwestern Yunnan. Beijing: Seismological Press, 321 (in Chinese).

Haddon, E., Amos, C.B., Zielke, O., Jayko, A.S., Bürgmann, R., 2016. Surface slip during large Owens Valley earthquakes. Geochemistry, Geophysics, Geosystems, 17(6), 2239–2269, doi: 10.1002/2015GC006033.

Han, Z.J., Dong, S.P., Tan, X.B., Mao, Z.B., Yuan, R.M., Hu, N., Guo, P., 2017. The Holocene activity and strike-slip rate of the southern segment of the Xiaojiang Fault in the southeastern Yunnan Region, China. Seismology and Geology, 39(1), 1–18 (in Chinese with English abstract).

Harrison, T.M., Copeland, P., Kidd, W.S.F., Yin, A., 1992. Raising Tibet. Science, 255 (5052), 1663–1670, doi:10.1126/science.255.5052.1663.

He, H.L., Yasutaka, I., He, Y.L., Togo, M., Chen, J., Chen, C.Y., Tajikara, M., Echigo, T., Okada, S., 2008. Newly-generated Daliangshan fault zone—Shortcutting on the central section of Xianshuihe-Xiaojiang fault system. Science in China Series D: Earth Sciences, 51(9), 1248–1258. https://doi.org/10.1007/s11430-008-0094-4.

He, H.L., & Oguchi, T., 2008. Late Quaternary activity of the Zemuhe and Xiaojiang faults in southwest China from geomorphological mapping. Geomorphology, 96(1–2), 62–85.

He, H.L., & Yasutakyr, I., 2007. Faulting on the Anninghe Fault Zone, Southwest China in Late Quaternary and its movement model. Acta Seismologica Sinica, 29(5), 537–548.

He, H.L., Ran, Y.K., Yasutaka I., 2006. Uniform Strike-Slip Rate along the Xianshuihe-Xiaojiang Fault System and Its Implications for Active Tectonics in Southeastern Tibet. Acta Geologica Sinica (English Version), 80(3), 376–386.

He, H.L., Song, F.M., Li, C.Y., 1999. Topographic survey of micro faulted landform and estimation of striking slip rate for the Zemuhe Fault, Sichuan Province. Seismology and Geology, 21(4), 361–369.

He, H.L., Yasutaka, I., Song, F.M., Dong, X.Q., 2002. Late Quaternary Slip Rate of the Xiaojiang Fault and its implication. Seismology and Geology, 24(1), 14–26.

Heritage, L.G., & Large, R.G.A., 2009. Laser Scanning for the Environmental Sciences. Blackwell Publishing Ltd, doi: 10.1002/9781444311952.

Huang, Z.Z., & Tang, R.C., 1983. The Zemuhe Fault and Earthquakes. Journal of Seismological Research, 6(2), 167–177 (in Chinese with English abstract).

Jiang, G.Y., Xu, X.W., Chen, G.H., Liu, Y.J., Fukahata, Y., Wang, H., Yu, G.H., Tan, X.B., Xu, C.J., 2015. Geodetic imaging of potential seismogenic asperities on the Xianshuihe-Anninghe-Zemuhe fault system, southwest China, with a new 3-D viscoelastic interseismic coupling model. Journal of Geophysical Research: Solid Earth, 120(3), 1855–1873.

Karabacak, V., Ring, U., Uysal, T.I., 2020. The off-fault deformation on the North Anatolian Fault zone and assessment of slip rate from carbonate veins. Tectonophysics, 795, 1–10. https://doi.org/10.1016/j.tecto.2020.228633.

Leloup, H.P., Lacassin, R., Tapponnier, P., Schärer, U., Zhong, D.L., Liu, X.H., Zhang, L.S., Ji, S.C., Trinh, T.P., 1995. The Ailao Shan–Red river shear zone (Yunnan, China), tertiary transform boundary of Indochina. Tectonophysics, 251(1–4), 3–84.

Leloup, P.H., Arnaud, N., Lacassin, R., Kienast, J.R., Harrison, T.M., Phan, T.T., Replumaz, A., and Tapponnier, P., 2001. New constraints on the structure, thermochronology and timing of the Ailao Shan–Red River shear zone, SE Asia. J. Geophys. Res., 106: 6657–6671.

Li, J.Y., Zhou, B.G., Li, T.M., Yang, Y.L., Li, Z.F., Long, F., 2020. Seismogenic depths of the Anninghe-Zemuhe and Daliangshan Fault Zones and their seismic hazards. Chinese J. Geophys, 63(10), 3669–3682 (in Chinese with English abstract), doi: 10.6038/cjg2020N0201.

Li, P., & Wang, L.M., 1975. Exploration of the seismo-geological features of the Yunnan-West Sichuan Region. Scientia Geological Sinica, 4, 308–326 (in Chinese with English abstract).

Li, T.S., Du Q.F., You, Z.L., Zhang, C.G., 1997. Xianshuihe active fault zone and strong earthquake risk assessment. Chengdu: Chengdu Cartographic Publishing House (In Chinese).

Li, Y.L., Wang, C.S., Zhao, X.X., Yin, A., Ma, C., 2012. Cenozoic thrust system, basin evolution, and uplift of the Tanggula Range in the Tuotuohe region, central Tibet. Gondwana Res, 22 (2), 482–492.

Liu, Y.H., Li, J., P., Wang, L.W., 2015. A study of crustal movement characteristics and seismic hazard of Xiaojiang Fault Zone. Engineering of Surveying and Mapping, 24(7), 58–61 (in Chinese with English abstract).

Loveless, J.P., & Meade, B.J., 2011. Partitioning of localized and diffuse deformation in the Tibetan Plateau from joint inversions of geologic and geodetic observations. Earth and Planetary Science Letters, 303(1–2), 11–24, doi:10.1016/j.epsl.2010.12.014.

Ma, H.F., 2019. Study on the fault slip rate and locking depth of Anninghe Fault. Journal of Geodesy and Geodynamics, 39(Supp. Ⅰ), 11–14 (in Chinese with English abstract).

McKenzie, D., & Jackson, J., 1986. A block model of distributed deformation by faulting. Journal of the Geological Society, 143, 349–353, doi: 10.1144/gsjgs.143.2.0349.

Meade, J.B., 2007. Algorithms for the calculation of exact displacements, strains, and stresses for triangular dislocation elements in a uniform elastic half space. Computers & Geosciences, 33(8), 1064–1075.

Molnar, P., & Tapponnier, P., 1975. Cenozoic tectonics of Asia: effects of a continental collision: features of recent continental tectonics in Asia can be interpreted as results of the India–Eurasia collision. Science, 189 (4201), 419–426.

Molnar, P., 1992. A review of seismicity, recent faulting and active deformation of the Tibetan Plateau. Journal of Himalayan Geology, 3(1), 43–78.

Molnar, P. & Lyon-Caen, H., 1989. Fault plane solutions of earthquakes and active tectonics of the Tibetan Plateau and its margins. Geophys. J. Int. 99, 123–153.

Pan, G.T., 2005. Geological map of Qinghai Tibet Plateau and its adjacent areas (1:1.5 million). Chengdu Institute of Geology and mineral resources, Ministry of land and resources, Sichuan Province.

Pei, X.Y., Wang, X.M., Zhang, C.G., 1997. Basic segmentation Characteristics on Late Quaternary Anninghe Active Faults. Earthquake Research in Sichuan, 4, 52–61 (in Chinese with English abstract).

Peltzer, G., & Tapponnier, P., 1988. Formation and evolution of strike-slip faults, rifts, and basins during the India-Asia collision: An experimental approach. Journal of Geophysical Research: Solid Earth, 93(B12), 15085–15117. https://doi.org/10.1029/JB093iB12p15085.

Peng, J.H., Liao, H., Gu, T., Zhang, Y., 2007. Motion characteristics of the Xianshuihe Fault based on observation data of GPS continuing-run reference stations. Earthquake Research in Sichuan, 4, 14–17 (in Chinese with English abstract) doi:10.3969/j.issn.1001–8115.2007.04.004.

Qian, H., Allen, R.C., Luo, Z.L., Wen, X.Z., Zhou, H.W., Huang, W.S., 1988. The Active Characteristics of Xianshuihe Fault in Holocene. Earthquake Research in China, 4(2), 9–18 (in Chinese with English abstract).

Qian, H., Tang, R.C., Wen, D.H., Huang, Z.Z., 1992. Research on the recent surfical faulting on the northern segment of the Anninghe Fault Zone and Earthquake Potential. Seismology and Geology, 14(4): 317–323 (in Chinese with English abstract).

Qiao, L., Yao, H.J., Lai, Y.C., Huang, B.S., Zhang, P., 2018. Crustal Structure of Southwest China and Northern Vietnam from Ambient Noise Tomography: Implication for the Large-Scale Material Transport Model in SE Tibet. Tectonics, 37. https://doi.org/10.1029/2018TC004957.

Qiao, X.J., Wang, Q., Du, R.L., 2004. Characteristics of current crustal deformation of active blocks in the Sichuan–Yunnan region. Chinese J. Geophys, 47(5), 805–811 (in Chinese with English abstract).

Ramsey, B.C., 1995. Radiocarbon Calibration and Analysis of Stratigraphy: The OxCal Program. Radiocarbon, 37(2), 425–430, doi: 10.1017/S0033822200030903.

Ran, Y.K., Cheng, J.W., Gong, H.L., Chen, L.C., 2008. Late Quaternary Geomorphic Deformation and Displacement Rates of the Anninghe Fault around Zimakua. Seismology and Geology, 30(1), 86–98 (in Chinese with English abstract).

Ren, J.W., 1990. Preliminary Study on the Recurrence Period of Strong Earthquakes on the Fracture Zone of Zemuhe, West of Sichuan. Inland Earthquake, 4(2), 107–115 (in Chinese with English abstract).

Replumaz, A. & Tapponnier, P., 2003. Reconstruction of the deformed collision zone between India and Asia by backward motion of lithospheric blocks. Journal of Geophysical Research: Solid Earth, 108(B6).

Roger, F., Calassou, S., Lancelot, J., Malavieille, J., Mattauer, M., Xu, Z., Hao, Z., Hou, L., 1995. Miocene emplacement and deformation of the Konga Shan granite (Xianshui He fault zone, west Sichuan, China): geodynamic implications. Earth Planet. Sci. Lett. 130, 201–216.

Royden, L.H., Burchfiel, B.C., King, R.W., Wang, E., Chen, Z.L., Shen, F., Liu, Y.P., 1997. Surface deformation and lower crustal flow in eastern Tibet. Science, 276(5313), 788–790, doi: 10.1126/science.276.5313.788.

Royden, L.H., Burchfiel, B.C., van der Hilst R.D., 2008. The geological evolution of the Tibetan Plateau. Science, 321(5892), 1054–1058, doi: 10.1126/science.1155371.

Shen, J., Wang, Y.P., Song, F.M., 2003. Characteristics of the active Xiaojiang fault zone in Yunnan, China: a slip boundary for the southeastward escaping Sichuan–Yunnan Block of the Tibetan Plateau. Journal of Asian Earth Sciences, 21(10), 1085–1096.

Shen, X.H., Chen, Z.W., Xu, R.D., Zhang, N., 2000. Deformation characteristics and displacement amount of the Liangshan Active Fault Zone in Late Cenozoic Era. Seismology and Geology, 22(3), 232–238 (in Chinese with English abstract).

Shen, Z.K., Lü, J.N., Wang, M., Burgmann, R., 2005. Contemporary crustal deformation around the southeast borderland of the Tibetan Plateau. Journal of Geophysical Research, v. 110, p. B11409, doi: 10.1029/2004JB003421.

Shen, Z.K., Wang, M., Li, Y., Jackson, D.D., Yin, A., Dong, D., Fang, P., 2001. Crustal deformation along the Altyn Tagh fault system, western China, from GPS. J. Geophys. Res., 106(B12):30607–30622, doi: 10.1029/2001JB000349.

Shi, F.Q., You, W., Fu, Y.W., 2012. Recent crustal movement characteristics of Xiaojiang River Fault Based on the GPS data. Journal of Seismological Research, 35(2), 207–213 (in Chinese with English abstract).

Shi, X.H., Sieh, K., Weldon R., Zhu, C.N., Han, Y., Yang, J.W., Robinson, W., S., 2018. Slip rate and rare large prehistoric earthquakes of the Red River fault, southwestern China. Geochemistry, Geophysics, Geosystems, 19(7), 2014–2031, doi: 10.1029/2017GC007420.

Shi, X.H., Wang, Y., Sieh, K., Weldon, R., Feng, L.J., Chan, C.H., Zeng, L.J., Fault Slip and GPS Velocities Across the Shan Plateau Define a Curved Southwestward Crustal Motion Around the Eastern Himalayan Syntaxis. Journal of Geophysical Research: Solid Earth, 123, 2502–2518. https://doi.org/10.1002/2017JB015206.

Song, F.M., Wang, Y.P., Yu, W.X., Cao, Z.Q., Shen, X.H., Shen, J., 1998. Xiaojiang Active Fault Zone. Beijing: Seismological Press (in Chinese).

Sun, H.Y., He, H.L., Wei, Z.Y., Gao, W., 2015. Late Quaternary activity of Zhuma Fault on the north segment of Daliangshan Fault Zone. Seismology and Geology, 37(2), 440–454 (in Chinese with English abstract).

Tang, R.C., Huang, Z.Z., Wen, D.H., Xia, D.D., 1989. A tentative study on the segmentation of the recent motions along the Anning River Fault and its relationship with Seismicity. Journal of Seismological Research, 12(4), 337–347 (in Chinese with English abstract).

Tang, R.C., Qian, H., Huang, Z.Z., Wen, D.H., Wu, X.G., Cai, C.X., Tian, H., 1992. The Feature of activity on the north segment of the Anninghe Fracture Zone since Late Pleistocene. Earthquake Research in China, 8(3), 60–68 (in Chinese with English abstract).

Tang, W.Q., Chen, Z.L., Liu, Y.P., Zhang, Q.Z., Zhao, J.X., Burchfiel, B.C., King, W.R., 2005b. Present-day tectonics activity in the intersection area of the Xianshuihe Fault and Longmenshan Fault on the eastern margin of the Qinghai-Tibet Plateau. Geological Bulletin of China, 24(12), 1169–1172 (in Chinese with English abstract).

Tang, W.Q., Liu, Y.P., Chen, Z.L., Huang, D.F., 2005a. GPS monitoring of Xianshuihe Fault and Blocks on its both sides. Journal of Southwest Jiaotong University, 40(3), 313–317 (in Chinese with English abstract).

Tang, W.Q., Liu, Y.P., Chen, Z.L., Zhang, Q.Z., Zhao, J.X., 2007. Monitoring of faults activity based on GPS. Journal of Mountain Science, 25(1), 103–107 (in Chinese with English abstract).

Tapponnier, P., & Molnar, P., 1977. Active faulting and tectonics in China. J. Geophys. Res. Solid Earth Planets 82 (20), 2905–2930.

Tapponnier, P., Peltzer, G., Le Dain, A.Y., Armijo, R., Cobbold, P., 1982. Propagating extrusion tectonics in Asia: New insights from simple experiments with plasticine. Geology, 10(12), 611–616.

Tzvetkov, J., 2018. Relief visualization techniques using free and open source GIS tools. Polish Cartographical Review, 50(2), 61–71.

Vosselman, G., & Mass, H., 2010. Airborne and Terrestrial Laser Scanning. UK: Whittles Publishing.

Wang, E., Burchfiel, C.B., Royden. H.L., Chen, L.Z., Chen, J.S., Li, W.X., Chen, Z.L., 1998. Late Cenozoic Xianshuihe-Xiaojiang, Red River, and Dali Fault Systems of Southwestern Sichuan and Central Yunnan, China. Geological Society of America, 327.

Wang, H., Wright, T.J., Biggs, J., 2009. Interseismic slip rate of the northwestern Xianshuihe Fault from InSAR data. Geophysical Research Letters, 36, L03302. https://doi.org/10.1029/2008GL036560.

Wang, H., Ran, Y.K., Chen, L.C., Liang, M.J., Gao, S.P., Li, Y.B., Xu, L.X., 2018. Deformation of slip rate on the Southern Segment of the Anninghe Fault. Seismology and Geology, 40(5), 967–979 (in Chinese with English abstract).

Wang, H., Ran, Y.K., Li, Y.B., 2011. Growth of a small pull-apart basin and slip rate of strike slip fault: with the example of Zemuhe Fault on the southeasten margin of the Tibetan Plateau. Seismology and Geology, 33(4), 818–827 (in Chinese with English abstract).

Wang, H., Ran, Y.K., Li, Y.B., Gomez, F., Chen, L.C., 2014. A 3400-year-long paleoseismologic record of earthquakes on the southern segment of Anninghe fault on the southeastern margin of the Tibetan Plateau. Tectonophysics, 628, 206–217.

Wang, M. & Shen, Z.K., 2020. Present-Day Crustal Deformation of Continental China Derived From GPS and Its Tectonic Implications. Journal of Geophysical Research: Solid Earth, 125(2), 1–22. https://doi.org/10.1029/2019JB018774.

Wang, S.F., Jiang, G.G., Xu, T.D., Tian, Y.T., Zheng, D.W., Fang, X.M., 2012. The Jinhe–Qinghe fault—An inactive branch of the Xianshuihe–Xiaojiang fault zone, Eastern Tibet. Tectonophysics, 544–545, 93–102.

Wang, W., Qiao, X.J., Yang, S.M., Wang, D.J., 2017b. Present-day velocity field and block kinematics of Tibetan Plateau from GPS measurements. Geophysical Journal International, 208(2), 1088–1102, doi: 10.1093/ gji/ggw445.

Wang, Y.Z., Wang, E.N., Shen, Z.K., Wang, M., Gan, W.J., Qiao, X.Y., Meng, G.J., Li, T.M., Tao, W., Yang, Y.L., Cheng, J., Li, P., 2008. GPS constrained inversion of present-day slip rates along major faults of the Sichuan–Yunnan region. China Science, ser. D, 51(9), 1267–1283, doi: 10.1007/s11430-008-0106-4.

Wang, Y.Z., Wang, M., Shen, Z.K., 2017a. Block-like versus distributed crustal deformation around the northeastern Tibetan plateau. Journal of Asian Earth Sciences, 140, 31–47.

Wei, W.X., Jiang, Z.S., Wu, Y.Q., Liu, X.X., Zhao, J., Li, Q., Dong, M., 2012a. Study on motion characteristics and strain accumulation of Xiaojiang Fault Zone. Journal of Geodesy and Geodynamics, 32(2), 11–15 (in Chinese with English abstract).

Wei, Z.Y., He, H.L., Shi, F., Xu, Y.R., Bi, L.S., Sun, H.Y., 2012b. Slip rate on the south segment of Daliangshan Fault Zone. Seismology and Geology, 34(2), 282–293 (in Chinese with English abstract).

Wells, D.L., & Coppersmith, K.J., 1994. New Empirical Relationships among Magnitude, Rupture Length, Rupture Width, Rupture Area, and Surface Displacement. Bulletin of the Seismological Society of America, 84, 974–1002.

Wen, X.Z., Allen, C.R., Luo Z.L., Qian, H., Zhou, H.W., Huang, W.S., 1989. Segmentation, geometric features, and their seismotectonic implications for the Holocene Xianshuihe Fault Zone. Earthquake Science, 11(4), 362–372 (in Chinese with English abstract).

Wen, X.Z., Du, F., Long, F., Fan, J., Zhu, H., 2011. Tectonic dynamics and correlation of major earthquake sequences of the Xiaojiang and Qujiang-Shiping fault systems, Yunnan, China. Science China Earth Sciences, 54(10), 1563–1575.

Wu, Z.H., & Zhou, C.J., 2018. Distribution map of active faults in China and its adjacent seas (1:5,000,000) and its specification. Beijing: Geological Publishing House.

Xiong, T.Y., Yao, X., Zhang, Y.S., 2010. A review on study of Xianshuihe Fault Zone since the Holocene. Journal of Geomechanics, 16(2), 176–188 (in Chinese with English abstract).

Xu, R., & Stamps, D.S., 2019. Strain Accommodation in the Daliangshan Mountain Area, Southeastern Margin of the Tibetan Plateau. Journal of Geophysical Research: Solid Earth, 124. https://doi.org/10.1029/2019JB017614.

Xu, X.W., Wen, X.Z., Zheng, R.Z., Ma, W.T., Song, F.M., Yu, G.H., 2003. The latest tectonic change patterns and power sources of active blocks in Sichuan-Yunnan area. Science in China (Series D), 33(Supp.), 151–162.

Yan, B., & Lin, A.M., 2017. Holocene activity and paleoseismicity of the Selaha Fault, southeastern segment of the strike-slip Xianshuihe Fault Zone, Tibetan Plateau. Tectonophysics, 694, 302–318.

Yan, B., & Lin, A.M., 2015. Systematic deflection and offset of the Yangtze River drainage system along the strike-slip Ganzi-Yushu-Xianshuihe Fault Zone, Tibetan Plateau. Journal of Geodynamics, 87, 13–25.

Yin, A., & Harrison, T.M., 2000. Geologic evolution of the Himalayan – Tibetan orogen. Annu. Rev. Earth Planet. Sci. 28, 211–280.

Yu, J.Q., 2010. Fault Activity Rate about Typical Sections of Zemuhe Fault Zone. Beijing, Institute of Forecasting, China Earthquake Administration, Master thesis (In Chinese with English abstract).

Zhang, K.Q., Wu, Z.H., Lv, T.Y., Feng, H., 2015. Review and progress of OSL dating. Geological Bulletin of China, 34(1): 183–203 (in Chinese with English abstract).

Zhang, P.Z., Shen, Z.K., Wang, M., Gan, W.J., Bürgmann, R., Molnar, P., Wang, Q., Niu, Z.J., Sun, J.Z., Wu, J.C., Sun, H.R., You, X.Z., 2004. Continuous deformation of the Tibetan Plateau from global positioning system data. Geology, 32(9), 809–812. https://doi.org/10.1130/G20554.1

Zhang, P.Z., 2013. A review on active tectonics and deep crustal processes of the western Sichuan region, eastern margin of the Tibetan Plateau. Tectonophysics, 584, 7–22. https://doi.org/10.1016/j.tecto.2012.02.021.

Zhang, P.Z., Li C.Y., Mao, F.Y., 2008. Strath terrace formation and strike slip faulting. Seismology and Geology, 30(1), 44–57 (in Chinese with English abstract).

Zhang, Y.S., Yao, X., Yu K., Du, G.L., Guo, C.B., 2016. Late-Quaternary slip rate and seismic activity of the Xianshuihe Fault Zone in Southwest China. Acta Geologica Sinica (English Edition), 90(2), 525–536.

Zhang, Y.Z., Replumaz, A., Leloup, P.H., Wang, G.C., Bernet, M., van der Beek, P., Paquette, J.L., Chevalier, L.M., 2017. Cooling history of the Gongga batholith: Implications for the Xianshuihe Fault and Miocene kinematics of SE Tibet. Earth and Planetary Science Letters, 465, 1–15.

Zheng, G., Wang, H., Wright, T.J., Lou, Y.D., Zhang, R., Zhang, W.X., Shi, C., Huang, J.F., Wei, N., 2017. Crustal Deformation in the India-Eurasia Collision Zone from 25 Years of GPS Measurements. Journal of Geophysical Research: Solid Earth, 122(11), 9290–9312.

Zhou, R.J., He, Y.L., Huang, Z.Z., Li, X.G., Y.T., 2001a. The slip rate and strong earthquake recurrence interval on the Qianning-Kangding segment of the Xianshuihe fault zone. Acta Seismologica Sinica (English Edition), 14(3), 263–273.

Zhou, R.J., He, Y.L., Yang, T., He, Q., Li, X.G., 2001b. Slip rate and strong earthquake rupture on the Moxi-Mianning segment along the Xianshuihe-Anninghe Fault Zone. Earthquake research in China, 17(3), 253–262 (in Chinese with English abstract).

Zhou, R.J., Li, X.G., Huang, Z.Z., He, Y.L., Ge, T.Y., 2003. Average slip rate of Daliang Mountain Fault Zone in Sichuan in Late Quaternary Period. Journal of Seismological Research, 26(2), 191–196 (in Chinese with English abstract).

Zielke, O., 2012. LaDiCaoz and lidar imager—MATLAB GUIs for lidar data handling and lateral displacement measurement. Geosphere, 8(1).

Zielke, O., Klinger, Y., Arrowsmith, J. R., 2015. Fault slip and earthquake recurrence along strike-slip faults — Contributions of high-resolution geomorphic data. Tectonophysics, 638, 43–62, doi: 10.1016/j.tecto.2014.11.004.